Riccardo Di Pietro, Tim Erdmann, Naixiang Wang, Xuhai Liu, David Gräfe, Johannes Lenz, Josef Brandt, Daniel Kasemann, Karl Leo, Mahmoud Al-Hussein, Kirill L. Gerasimov, David Doblas, Dimitri A. Ivanov, Brigitte Voit, Dieter Nehera, Anton Kiriy

The impact of molecular weight, air exposure and molecular doping on the charge transport properties and electronic defects in dithienyldiketopyrrolopyrrole- thieno[3,2-b]thiophene copolymers

Erstveröffentlichung in / First published in:
Journal of Materials Chemistry C. 2016, 4(46), S. 10827 - 10838 [Zugriff am: 04.11.2019]. Royal Society of Chemistry. ISSN 2050-7534.

DOI: https://doi.org/10.1039/c6tc03545k

Journal of Materials Chemistry C

PAPER

View Article Online
View Journal | View Issue

Cite this: J. Mater. Chem. C, 2016, 4, 10827

The impact of molecular weight, air exposure and molecular doping on the charge transport properties and electronic defects in dithienyl-diketopyrrolopyrrole-thieno[3,2-*b*]thiophene copolymers†

Riccardo Di Pietro,‡*[a] Tim Erdmann,[bc] Naixiang Wang,[a] Xuhai Liu,[d] David Gräfe,[bc] Johannes Lenz,[b] Josef Brandt,[b] Daniel Kasemann,[d] Karl Leo,[cd] Mahmoud Al-Hussein,[e] Kirill L. Gerasimov,[f] David Doblas,[f] Dimitri A. Ivanov,[fg] Brigitte Voit,[bc] Dieter Neher[a] and Anton Kiriy*[bc]

Received 16th August 2016,
Accepted 13th October 2016

DOI: 10.1039/c6tc03545k

www.rsc.org/MaterialsC

We performed an in-depth study of high molecular weight poly[3,6-(dithiophene-2-yl)-2,5-di(2-octyldodecyl)-pyrrolo[3,4-*c*]pyrrole-1,4-dione-*alt*-thieno[3,2-*b*]thiophene] P(DPP2OD-TT) synthesized through the Stille coupling polycondensation in order to understand the correlation between molecular weight, processing conditions and charge transport. We observed a rapid increase in its aggregation in solution with increasing molecular weight which strongly limits the solubility and processability for weight average molecular weights beyond 200 kg mol^{-1}. This results in severe limitation in the charge transport properties of the polymer. We further observe the presence of bulk electronic defects in all different polymer batches that severely limit the current flow and manifest themselves in organic field effect transistors as apparent charge density dependence of the mobility. These defects are passivated by exposure to an ambient atmosphere, as confirmed by an increase in current and mobility that is no more charge density dependent. This is further confirmed by the result of chemical doping using 2,2-(perfluoronaphthalene-2,6-diylidene)dimalononitrile, F_6TCNNQ, which leads to the filling of the trap states and a higher charge density independent mobility of up to 1 cm^2 V^{-1} s^{-1}.

Introduction

Solution-processable conjugated polymers have attracted great interest in the past decade as basic semiconductor materials for various flexible electronic devices such as organic field-effect transistors (OFETs) and organic solar cells (OPVs).[1–4] Recent developments have led to a dramatic progress in the performance of OFETs based on polymeric semiconductors, with reports of remarkably high field-effect mobilities.[5–8] One of such classes of polymeric semiconductors are dithienyl-diketopyrrolopyrrole (DPP)-based polymers;[9,10] since the demonstration of a promising charge carrier mobility in poly[3,6-bis-(4′-dodecyl-[2,2′]bithiophenyl-5-yl)-2,5-bis-(2-ethyl-hexyl)-2,5-dihydropyrrolo[3,4]-pyrrole-1,4-dione] (pBBTDPP2) in 2008,[11,12] a number of other DPP polymers exhibiting mobilities in the range of 0.1–10 cm^2 V^{-1} s^{-1} have been synthesized and tested.[9] The copolymer P(DPP2OD-TT) comprising alternating DPP and thieno[3,2-*b*]thiophene (TT) moieties (Chart 1) is one of the most promising DPP based organic semiconductors due to its reported record hole mobility of up to 10 cm^2 V^{-1} s^{-1}.[6] This polymer structure (named PDBT-*co*-TT) was first introduced

[a] Institute of Physics and Astronomy, University of Potsdam (Uni Potsdam), Karl-Liebknecht-Str. 24-25, 14476 Potsdam, Germany. E-mail: Riccardo.dipietro@hitachi-eu.com
[b] Leibniz-Institut für Polymerforschung Dresden e.V. (IPF), Hohe Straße 6, 01069 Dresden, Germany. E-mail: kiriy@ipfdd.de
[c] Technische Universität Dresden, Center for Advancing Electronics Dresden (cfaed), 01062, Dresden, Germany
[d] Technische Universität Dresden, Institut für Angewandte Photophysik (IAPP), George-Bähr-Straße 1, 01069 Dresden, Germany
[e] The University of Jordan, Physics Department, Amman 11942, Jordan
[f] Lomonosov Moscow State University, Faculty of Fundamental Physical and Chemical Engineering, GSP-1, 1-51 Leninskie Gory, Moscow, 119991, Russia
[g] Institut de Sciences des Matériaux de Mulhouse, CNRS UMR 7361, 15, Jean Starcky, F-68057, Mulhouse, France

† Electronic supplementary information (ESI) available: Monomer synthesis; the NMR spectrum of the polymer; GPC plots; TGA, DSC, and CV results; 2D GIWAXS patterns of P2 and P3 and thick film XRD and GIWAXS measurements. See DOI: 10.1039/c6tc03545k

‡ Current address: Hitachi Cambridge Laboratory, Cavendish Laboratory, J. J. Thomson Avenue, CB3 0HE Cambridge, UK.

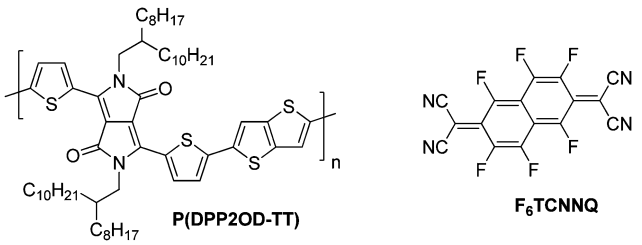

Chart 1 Molecular structure of the polymer P(DPP2OD-TT) and the molecular dopant F_6TCNNQ.

in 2010 by Li *et al.*[13] In that work, bottom gate top contact (BGTC) transistors fabricated using P(DPP2OD-TT) with a moderate molecular weight (weight-average molecular weight, M_w = 210 kg mol^{-1}, PDI = 2.36 (GPC solvent THF)) exhibited a hole mobility of about 1 cm^2 V^{-1} s^{-1}. In 2011, Zhang *et al.* reported a series of DPP-based polymers among which P(DPP2OD-TT) (M_w = 39 kg mol^{-1}, PDI = 2.6 (GPC solvent chlorobenzene)) showed a saturation hole mobility of 0.38 cm^2 V^{-1} s^{-1} for transistors fabricated on silanized substrates and annealed at 150 °C.[14] Sirringhaus *et al.* reinvestigated the charge transport properties of P(DPP2OD-TT) with the aim of achieving ambipolar switching using a P(DPP2OD-TT) polymer (M_w = 190 kg mol^{-1}, PDI = 3.87, GPC solvent not mentioned).[15] By tuning the work function of the metal electrodes for achieving efficient injection of both charge carrier types, they demonstrated P(DPP2OD-TT) OFETs with balanced hole and electron mobilities both on the order of 1 cm^2 V s^{-1}. In all these works, morphological studies revealed high thin-film crystallinity and a packing structure with edge-on oriented polymer chains, a lamellar *d*-spacing of ≈20 Å and a π–π stacking distance of ≈3.8 Å, a morphology particularly favorable for charge transport parallel to the substrate.

In 2012, Ong *et al.* reported a remarkable hole mobility of above 5 cm^2 V^{-1} s^{-1} for the P(DPP2OD-TT) batch having extremely high molecular weight (M_w = 501 kg mol^{-1}) as measured by GPC in 1,2,4-trichlorobenzene at 160 °C.[16] The exceptionally high transistor performance of the highest molecular weight P(DPP2OD-TT) was correlated with its ability to form films with a closer crystal packing than that of the lower molecular weight samples. In their work annealed P(DPP2OD-TT) films exhibited a lamellar *d*-spacing of 18.4 Å and a π–π stacking distance of 3.43 Å, values that are substantially smaller than those reported in previous papers.[16]

The good charge transport properties are generally correlated to the high degree of crystallinity of the polymer films, without addressing the specific role played by single elements such as chain length or crystallite size. It has been reported by several research groups that the increase of the molecular weight improves charge transport in conjugated polymers because longer chains serve as better pathways for charges across crystalline domains than shorter ones.[16,17] However, high molecular weight polymers may also suffer from insufficient solubility and a high degree of chain entanglement which in turn may reduce the film crystallinity and worsen the charge transport properties, as observed in another DA copolymer – high electron mobility P(NDI2OD-T2) – as well as in poly(3-hexylthiophene) (P3HT).[18,19] Furthermore, morphological effects should be carefully separated from the role played by air exposure in charge transport. In the cited works measurements have been performed either in an inert[12,13,17] or ambient atmosphere[11,15] supporting the general claim for the environmental stability of the polymer but without checking in detail what differences are observed upon air exposure, which might limit the possibility to compare results of different works. Comparison of polymer batches obtained from different labs is also made difficult due to inaccuracies in the electrical parameters extraction and the low reproducibility of the GPC analysis, due to the strong aggregation tendency of DPP polymers which leads to artificially inflated values, expecially when measuring at low temperatures.[16,20]

Here we discuss the charge transport properties of three different batches of high molecular weight P(DPP2OD-TT) (Chart 1) prepared by the Stille polycondensation. We show that for a weight average molecular weight (M_w) in excess of 200 kg mol^{-1} pre-aggregation in solution limits both solubility and processability. We also study in detail the effect of air exposure on the electrical characteristics of the device and show that the effect is similar to what is observed upon chemical doping of the polymer film with F_6TCNNQ (Chart 1). These results allow us to determine that air exposure has no direct impact on charge transport in the active area of the transistor but is rather responsible for trap passivation in the bulk of the polymer film, where charge density is much lower. Such an improvement in bulk transport manifests itself as strong enhancement of the hole injection process. These results provide useful insights into the limiting factors for DPP based OFET performance and highlight possible ways to overcome these issues and improve device performance for potential use in logic circuit applications.

Experimental section

Materials and syntheses

F_6TCNNQ was purchased from Novaled GmbH; all other chemicals and solvents were ordered from Sigma Aldrich, Acros Organics, ABCR and TCI and used as received.

Typical Stille's polycondensation procedure for P(DPP2OD-TT)s. Under a nitrogen atmosphere, 204 mg (0.20 mmol, 1.0 eq.) of 3,6-bis(5-bromothiophene-2-yl)-2,5-bis(2-octyldodecyl)pyrrolo[3,4-*c*]-pyrrole-1,4(2*H*,5*H*)-dione, 93 mg (0.20 mmol, 1.0 eq.) of 2,5-bis(trimethylstannyl)-thieno[3,2-*b*]thiophene, 3.7 mg (4 μmol, 0.02 eq.) of tris(dibenzylideneacetone)dipalladium(0) and 4.9 mg (16 μmol, 0.08 eq.) of tri(*o*-tolyl)phosphine were dissolved in 40 ml degassed, anhydrous chlorobenzene. The solution was placed into a preheated oil bath, stirred for 3 days at 130 °C, precipitated in conc. HCl/MeOH (8 ml/100 ml), stirred overnight and the collected solids were purified *via* Soxhlet extraction using methanol, acetone, hexane, and DCM. The final chloroform fraction was washed with 50 ml of aqueous sodium *N*,*N*-diethyldithiocarbamate solution ($c \sim 10$ g l^{-1}) for 2 h at 60 °C and at room temperature 4 times with water afterwards. The polymer was isolated by precipitation in methanol, filtration

and drying in a vacuum at 40 °C resulting in a dark solid. ^{1}H-NMR ($C_2D_2Cl_4$, 393 K, 500 MHz) δ [ppm] = 9.07 (br. s.), 7.20 (br. s.), 4.10 (br. s.), 2.12 (br. s.), 1.44 (br. s.), 0.96 (br. s.) (see Fig. S1, ESI†). Three different batches were prepared following this synthetic procedure, differing only in molecular weight.

P1: yield: 89%. GPC ($CHCl_3$, 313 K): M_n = 255.0 kg mol^{-1}, M_w = 720.0 kg mol^{-1}, PDI = 2.83. HT-GPC (1,2,4-trichlorobenzene, 423 K): M_n = 52.0 kg mol^{-1}, M_w = 177.0 kg mol^{-1}, PDI = 3.40.

P2: yield: 90%. GPC ($CHCl_3$, 313 K): M_n = 253.0 kg mol^{-1}, M_w = 1022.0 kg mol^{-1}, PDI = 4.04. HT-GPC (1,2,4-trichlorobenzene, 423 K): M_n = 70.0 kg mol^{-1}, M_w = 222.0 kg mol^{-1}, PDI = 3.17.

P3: yield: 91%. GPC ($CHCl_3$, 313 K): M_n = 410.0 kg mol^{-1}, M_w = 1371.0 kg mol^{-1}, PDI = 3.34. HT-GPC (1,2,4-trichlorobenzene, 423 K): M_n = 59.0 kg mol^{-1}, M_w = 227.0 kg mol^{-1}, PDI = 3.90.

Instrumentation

Nuclear magnetic resonance (NMR) spectroscopy. ^{1}H (500.13 MHz) and ^{13}C (125.75 MHz) NMR spectra were recorded using a Bruker DRX 500 spectrometer and $CDCl_3$/DMSO-d_6/$C_2D_2Cl_4$ as solvents. The NMR spectra were referenced to the residual non-deuterated solvent signal (^{1}H-NMR: 7.26 ppm/2.50 ppm/5.98 ppm, ^{13}C-NMR: 77.16 ppm/39.52 ppm/not measured).

Gel permeation chromatography (GPC). GPC measurements were carried out on a PL-GPC 50 Plus (Polymer Laboratories, USA) normal-temperature size exclusion chromatograph, equipped with UV/Vis and refractive index detectors and a three-column system (precolumn ResiPore and first/second main column Resipore/PLgel 5 μm Mixed-C). Chloroform was used as an eluent at 40 °C and 1 ml min^{-1} flow rate. The number and weight average molecular weights (M_n, M_w) and polydispersities (PDI = M_w/M_n) were determined based on calibration with polystyrene standards obtained from Polymer Standards Service (PSS, Germany).

High temperature GPC (HT-GPC). HT-GPC measurements against polystyrene standards were performed using a PL-GPC 220 (Polymer Laboratories, USA) with two MIXED-B-LS columns and 1,2,4-trichlorobenzene as an eluent at 150 °C and 1 ml min^{-1} flow rate. Samples (2.5–3.0 mg ml^{-1}) were dissolved at 150 °C for at least 7 h, cooled to 80 °C and heated again up to 150 °C for 2 h prior to each individual measurement.

Matrix-assisted laser desorption/ionization time-of-flight mass spectrometry (MALDI-TOF-MS). MALDI-TOF mass spectra were recorded on an Autoflex Speed MALDI-TOF-/TOF-TOF-System (Bruker, USA) in a reflector mode with a Smartbeam laser (modified Nd:YAG laser). Samples were prepared from THF solutions (1 mg ml^{-1}) using dithranol as a matrix (10 mg ml^{-1} in THF). Equal amounts of both solutions were mixed and spotted on the MALDI plate.

Thermogravimetric analysis (TGA). TGA scans were carried out using a TA Instruments Q5000 at a heating rate of 10 K min^{-1} under a nitrogen gas flow.

Differential scanning calorimetry (DSC). For DSC measurements a TA Instruments Q1000 was used at a scan rate of 10 K min^{-1} and under a nitrogen atmosphere.

Cyclic voltammetry (CV). CV measurements were performed under a nitrogen atmosphere in a deoxygenated solution of tetra-*n*-butylammonium hexafluorophosphate in anhydrous acetonitrile (0.1 M). The three-electrode setup consisted of a non-aqueous Ag/Ag$^+$ reference electrode, a platinum wire as an auxiliary electrode and a platinum disc working electrode which was freshly coated by a thin film of the polymer sample prior to every measurement. The voltammograms were recorded at 50 mV s^{-1} and referenced to the signal of the ferrocene/ferrocenium redox couple as an external standard. HOMO energies were calculated according to the equation $E_{HOMO} = -(5.09 + E_{onset,ox\ vs.\ Fc/Fc^+})$ [eV].[21]

UV-Vis and charge accumulation spectroscopy. Both measurements have been performed using a Varian Cary 5000 spectrometer. Solution spectra have been acquired at low concentrations (0.01 g l^{-1}) to limit the formation of aggregates. Charge accumulation spectroscopy (CAS) has been performed on the same instrument using a custom-made sample holder in a nitrogen atmosphere. Drain contact was biased with a Keithley 2400 source measure unit, while the gate contact was biased using a Keithley 230 voltage source.

X-ray diffraction. Grazing incidence wide-angle X-ray measurements (GIWAXS) of ~1 μm thick films of P1 were performed using a Bruker D8 Discover diffractometer operating at 1.6 kW. The diffractometer is equipped with a Cu twist tube, a Ni filter (λ = 1.5418 Å), a Goebel mirror, and a 0.3 mm PinHole collimator for the incident beam. The sample was mounted on an Eulerian Cradle with an automatic controlled X–Y–Z stage. The GIWAXS patterns were recorded using a VÅNTEC-500 area detector using a sample-to-detector distance of 105 mm and an incident angle of 0.5°. High resolution specular data were obtained using a 2-circle diffractometer (XRD 3003 T-T, Seifert-FPM) and a point detector. By employing a parabolic multilayer mirror, a highly parallel beam of monochromatic Cu-K$_\alpha$ radiation (λ = 1.5418 Å) was obtained.

The GIWAXS experiments were also performed for thin (~50 nm) films prepared by spin-coating of polymers P1, P2 and P3. These films were investigated at the ID-10 beamline of the European Synchrotron Radiation Facility (Grenoble, France). The 2D diffraction patterns were collected with a Pilatus 300k detector (172 × 172 μm^2 pixel size). The wavelength used was 1.24 Å. The measurements were performed on thin films deposited on Si substrates at an incidence angle of 0.2 deg. The modulus of the scattering vector q was calibrated using several diffraction orders of silver behenate. *In situ* heating ramps were performed with a Linkam heating stage. The data correction and reduction was performed with home-made routines written in Igor Pro software.

Field-effect transistors (University of Potsdam). P(DPP2OD-TT) samples were characterized by using either bottom contact top-gate (BCTG) or top contact bottom gate (TCBG) OFETs. For BCTG transistors chromium (1.5 nm)/gold (30 nm) source–drain electrodes were deposited on the surface of standard cleaned glass substrates through shadow mask evaporation. Before deposition of the semiconductor, the substrates with gold electrodes were cleaned in an ultrasonic bath by using chloroform, acetone and isopropanol, each for 5 min. In the case of TCBG n-doped silicon substrates with thermal oxide

(300 nm thick) were used, cleaned in an ultrasonic bath using acetone and isopropanol. The surface was further cleaned by immersion in a piranha etching solution for 5 min and subsequent O_2 plasma etching for 2 min. The dielectric interface was then functionalized with an octyl-trichlorosilane (OTS) self-assembled monolayer, obtained by exposing the substrates to OTS vapors in a desiccator at 180 °C for 3 h. After that, P(DPP2OD-TT) dissolved under nitrogen (glovebox) either in dichlorobenzene (DCB) or 1-methylnaphthalene (1-MN) was spin-coated on the pre-cleaned substrates at 1000 rpm for 60 s at room temperature, yielding a semiconductor layer with a thickness of 20–60 nm. To further tune the transistor performance the devices were then either dried in a vacuum oven (as cast) or annealed at 100, 200 and 300 °C, respectively, for 20 min under nitrogen. For BCTG devices, electronic grade PMMA (M_n = 300 kg mol^{-1}, polymer source, 60 mg/ml in butyl acetate) was spin-coated on top of the annealed films at 1200 rpm for 90 s, yielding a dielectric layer with a thickness of 500 nm, and then heated at 80 °C for 20 min to remove the remaining solvent from the film. Al gate electrodes were deposited with a thickness of 20 nm. For TCBG devices, 30 nm thick gold electrodes were instead deposited *via* shadow mask evaporation. All the devices have the same channel length (L = 100 μm) and channel width (W = 149 mm).

Field-effect transistors (Institut für Angewandte Photophysik (IAPP)). Cr/Au (2 nm/30 nm) source and drain electrodes were fabricated on pre-cleaned glass substrates in a single-chamber ultra-high vacuum (UHV) tool (Kurt J. Lesker Company) at a base pressure of 10^{-6} mbar. The transistors were patterned by shadow masks with a channel length of 300 μm and a total channel width of 20 mm. The samples were transferred to a N_2 glovebox (H_2O < 0.1 ppm, O_2 < 0.1 ppm), and a P(DPP2OD-TT) solution (4 mg ml^{-1} in chloroform) was spin-coated onto the glass substrate through a 0.45 μm filter at 1000 rpm for 60 s, resulting in a thickness of 55 nm, as determined by a Dektak profilometer. The samples were then transferred to an UHV system and thin layers of (2,2-(perfluoronaphthalene-2,6-diylidene)dimalononitrile), F_6TCNNQ (Chart 1), (1–3 nm), were deposited on top of P(DPP2OD-TT) at a rate of 0.1 Å s^{-1}. The samples were again transferred to the N_2 glovebox, and multilayers of Cytop CTL-809M, dissolved in CT-Solv.180 at a ratio of 3 : 8, were spin-coated onto each sample at 500 rpm for 10 s followed by 1000 rpm for 20 s and subsequently dried on a hotplate for 30 minutes at 90 °C. The resulting thickness of the multi-layer Cytop was 900 (±20) nm. The samples covered by the polymer dielectric were transferred back to the UHV chamber and a 35 nm Al top gate was deposited through a shadow mask. The transistor output and transfer characteristics were measured in a N_2 atmosphere using a HP4145B semiconductor parameter analyzer. The sample transfer was done without exposing them to ambient air.

Results and discussion

Synthesis

According to the work of Ong *et al.*, high molecular weight P(DPP2OD-TT) (Chart 1) was prepared by the Stille polymerization conducted for 72 h in chlorobenzene at 130 °C in the presence of a Pd(0) source tris(dibenzylideneacetone)dipalladium(0) and a phosphine ligand tri(*o*-tolyl)phosphine, whereas other catalysts and lower boiling point solvents resulted in lower molecular weight polymers.[16] It must however be noted that the proposed reaction conditions are rather standard for the preparation of high molecular weight donor–acceptor copolymers by the Stille polycondensation method. With the aim of achieving high molecular weight polymers, the synthetic protocol by Ong *et al.* was used to synthesize three P(DPP2OD-TT) batches.[16] Furthermore, we conducted washings with a palladium scavenger, proposed as an additional purification step.[22–26] The crude copolymer mixtures, prepared in three independent polymerization runs, were separated into different molecular weight fractions by Soxhlet extraction with different solvents. Low molecular weight fractions extracted by acetone, hexane and CH_2Cl_2 in all three batches constituted minor fractions which were not used. All the polymer batches show high temperature stability (5% weight loss above 390 °C) as determined by thermogravimetric analysis (TGA) (Fig. S4, ESI†). In differential scanning calorimetry (DSC) scans conducted up to 350 °C a melting transition was observed starting at about 320 °C, but could not be recorded completely. In the cooling run and second heating scan phase transitions were not detected (Fig. S5, ESI†). On performing DSC heating scans up to the decomposition temperature melting occurred at about 370 °C. The major fractions of the polymers were soluble in boiling chloroform, in contrast to the paper of Ong *et al.* where the predominant fraction of the polymer (56%) was insoluble in chloroform but soluble in boiling chlorobenzene.[16] This may suggest that our polymers have a somewhat lower molecular weight than the highest molecular weight polymer obtained in their work. Because donor–acceptor copolymers tend to strongly aggregate in solution which affects the determination of molecular weight, GPC measurements were performed at elevated temperatures in chlorinated solvents (in chloroform at 40 °C and in 1,2,4-trichlorobenzene (TCB) at 150 °C).[27]

The results of GPC measurements reported in Table 1 reveal that all P(DPP2OD-TT) batches exhibit several times higher molecular weights in chloroform at 40 °C than the ones found upon measurement in TCB at 150 °C indicating strong aggregation at low temperatures (Fig. S2 and S3, ESI†). The P(DPP2OD-TT) sample further denoted as P1 shows the lowest molecular weight with M_w = 177 kg mol^{-1}. P2 and P3 have substantially higher M_w of 222 and 227 kg mol^{-1}, respectively. A closer comparison of the molecular weights obtained in chloroform and TCB shows that the lower molecular weight batch P1 displays the lowest aggregation in $CHCl_3$. It dissolves much faster, *i.e.*,

Table 1 Molecular weights of different P(DPP2OD-TT) batches as determined by GPC based on calibration with PS standards

	In $CHCl_3$ at 40 °C			In TCB at 150 °C		
Sample	M_w	M_n	PDI	M_w	M_n	PDI
P1	720	255	2.8	177	52	3.4
P2	1022	253	4.0	222	70	3.2
P3	1371	410	3.3	227	59	3.9

within about 15 minutes, in chloroform or dichlorobenzene upon agitation at elevated temperatures, and its solution can be easily filtered through a Teflon filter with a pore size of 400 nm. In contrast, the two other batches require a much longer time for complete dissolution and their solutions do not pass through the 400 nm-pore filter. Despite the molecular weights measured for the three polymer batches we have synthesized being about half of what had been reported by Ong *et al.* we found that solubility decreases dramatically for $M_w > 200$ kg mol^{-1}, where even a slight increase in molecular weight (from P2 to P3) leads to a dramatic increase in aggregation (as seen from GPC in $CHCl_3$).[16]

Absorption spectroscopy

UV-Vis spectroscopy was used to investigate further the aggregation behavior of different P(DPP2OD-TT) polymer batches. The absorption spectra in solution (Fig. 1a) show a very similar absorption spectra for P1 and P2 with a strongly enhanced low energy peak at 1.50 eV and a shoulder at 1.65 eV, despite the very low concentration of 10 μg ml^{-1}, and regardless of the chosen high boiling point solvent (we used dichlorobenzene, DCB, and 1-methylnaphthalene, 1-MN). This is consistent with a strong J-aggregate behavior already observed in solution.[28] In thin films however (Fig. 1b and c) the absorption is slightly blue-shifted, with the high energy shoulder (at 1.67 eV) more intense than the low energy peak (at 1.55 eV) for both P1 and P2 (films were prepared from solutions with a 5 g l^{-1} concentration). In the framework of H- and J-polymer aggregates this effect can be explained by the presence of amorphous domains and the formation of aggregates with a much stronger interchain coupling and a shorter intrachain extension of the electronic orbitals compared to the aggregates observed in solution. The spectrum is therefore a combination of more elongated J-aggregates already present in solution combined with smaller and more disordered aggregates that are formed during spin coating. When comparing P1 and P2 (Fig. 1d), one can observe a much more pronounced higher energy absorption in the case of P2 indicating a higher fraction of poorly aggregated and non-aggregated species in the film, possibly indicating that the higher M_w in this case might be detrimental to film formation. In both cases, however, the thin film UV-Vis spectrum shows an increase of the low energy transition compared to the high-energy one upon annealing, indicating the enlargement of polymer aggregates and the improvement of backbone planarization (Fig. 1b and c). The polymer P3 however displays a markedly different behavior: the solution

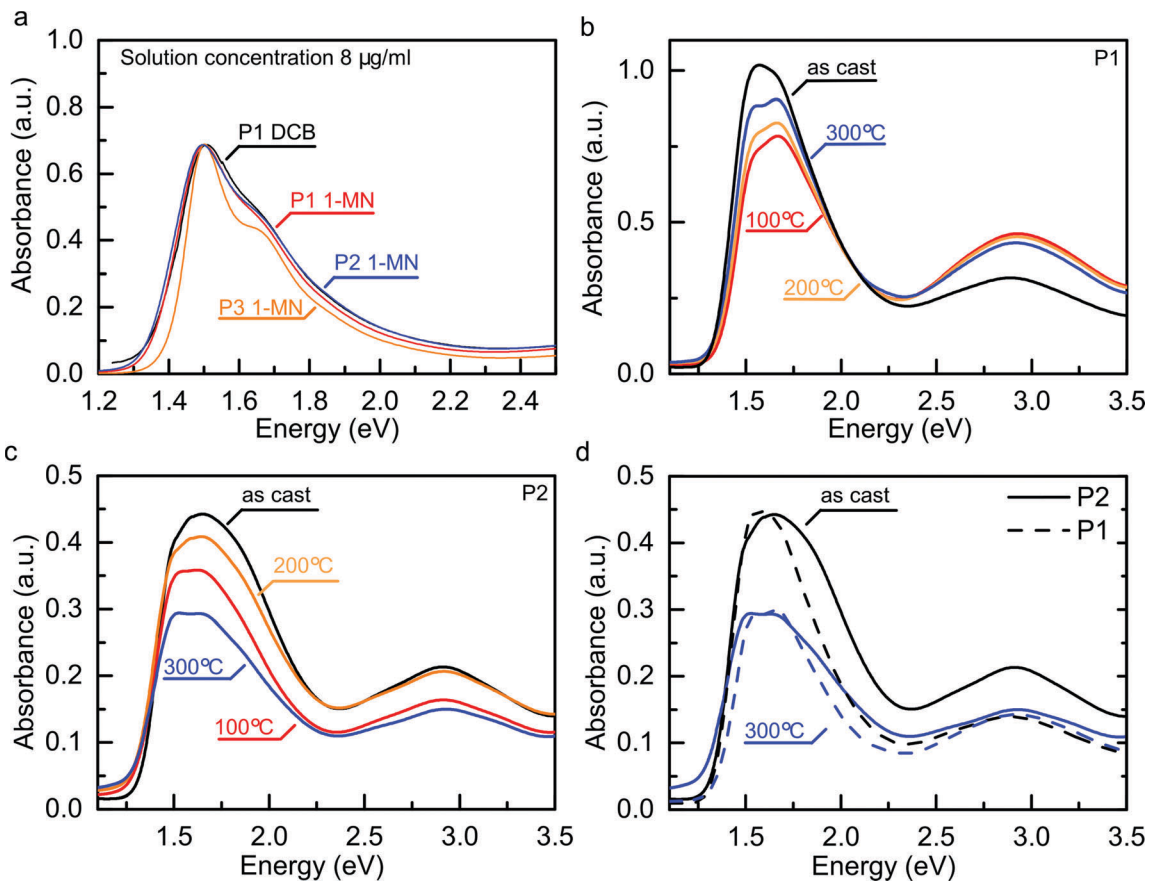

Fig. 1 (a) Solution spectra of P1 and P2 in different solvents, showing rather similar aggregation behaviour in solution independent of the chosen solvent; (b and c) thin film absorption spectra of P1 and P2, respectively, dissolved in 1-methylnaphthalene (1-MN), annealed at different temperatures (the as-cast sample is dried in a vacuum at RT to remove any residual solvent after spin coating); and (d) a comparison of thin film spectra of P1 and P2, as-cast and annealed at 300 °C (rescaled to highlight the spectral changes in the absorption spectrum).

absorption spectrum in 1-MN shows much sharper absorption peaks, with the high energy peak at 1.50 eV much stronger than the shoulder at 1.65 eV compared to the other two polymers. However, due to much stronger aggregation, P3 does not fully dissolve in high boiling point solvents at room temperature. This resulted in the fact that it is not possible to prepare films of P3 dissolved in 1-MN, due to the solution being highly viscous and leading to non-uniform films with undissolved polymer particles observable with the naked eye.

X-Ray diffraction

Further insights into the film formation mechanisms can be obtained through grazing incidence WAXS measurements, performed on thin films of P1, P2 and P3 using a synchrotron-based instrument at the ID10 beamline of the ESRF. In order to compare the properties of the three polymer batches, films were fabricated by spin-coating from chloroform to have a thickness of about 50 nm. The 2D diffractograms corresponding to the as-cast films and the films annealed at 200 °C of P1 are presented in Fig. 2a and b (the data for P2 and P3 are reported in the ESI,† Fig. S6). For all the different materials it can be seen that already the as-cast films reveal one strong reflection (the 100 diffraction peak) positioned along the meridional direction of the patterns, which corresponds to a population of crystalline domains oriented edge-on on the substrate. However, a diffraction peak pertinent to the π–π stacking is also observed along the same direction, which indicates that the sample contains not only edge-on oriented crystals but also a crystal population with a flat-on orientation of the molecular planes. Considering the fact that chloroform leads to very fast drying kinetics and usually leads to a rather disordered morphology, high crystallinity is a strong sign of very large aggregation taking place in solution.[19]

Upon annealing, the diffraction patterns of three different polymers undergo a significant and similar change: the patterns in the meridional direction start to exhibit higher orders of diffraction of the 100 peak (*cf.* Fig. 2c and d), which indicates that structural reorganization occurs during the high-temperature treatment that reduces the disorder and increases the size of the crystalline domains. The azimuthal profiles of the diffracted intensity provide further information on the nature of the process. The azimuthal distribution of the 100 intensity in Fig. 2e, g and i for P1, P2 and P3, respectively, becomes much more focused along the meridional direction and centered in a single peak, indicating an enhancement of the edge-on population of the crystals.

This observation is further corroborated by the azimuthal profile of the 010 peak (*cf.* Fig. 2f, h and l): for this diffraction peak the intensity along the meridional direction is strongly reduced upon annealing, while the peak intensity along the equatorial direction is increased, again consistent with a structural reorganization increasing the edge-on crystallite population. Similar conclusions can also be extracted from the XRD and GIWAXS analyses of free-standing thick polymer films (1 μm), which are reported in the ESI† (Fig. S7). From these measurements a lamellar stacking distance of 20.7 Å and a π–π stacking distance of 3.9 Å can be extracted. These data corroborate well with the data from Chen and Sirringhaus *et al.*,[15] Li and Sonar *et al.*[13] and Zhang and Toney *et al.*,[14] but not with Ong *et al.*[16] who reported a lamellar d spacing of 18.4 Å and an exceptionally short π–π stacking distance of 3.43 Å.

Looking in more detail at the differences between different polymers, P1 shows somewhat narrower 100 peaks, which infers a larger crystal size along this direction. Furthermore, a close inspection of the angular distribution of the 010 diffraction peak of three different films reveals how the reorientation from face-on to edge-on crystallites upon annealing is more efficient for P1 than for P2 and P3; while P1 shows strongly decreased peak intensity along the meridional direction upon annealing; for the other two polymers such conversion is not so efficient, strongly suggesting the presence of a less ordered and uniform texture in the high molecular weight polymers due to the stronger aggregation and lower solubility.

Transistor characterization (University of Potsdam)

The semiconducting properties of P(DPP2OD-TT) samples were characterized using BCTG and TCBG transistor configurations. If not stated otherwise, OFETs were fabricated and measured in a glovebox under a nitrogen atmosphere. All the devices based on both the lower molecular weight P1 and the higher molecular weight P2 polymer batches showed a typical p-channel transistor behavior. In Fig. 3a and b an example of the typical output and transfer characteristics is shown (the semiconducting layer in this case is P1 dissolved in dichlorobenzene and annealed at 300 °C).

The plot of the square root of the saturation current *versus* gate voltage (Fig. 4b) shows a deviation from a linear slope at low gate voltages, which can be due to a number of effects including the gate voltage dependent mobility or the effect of contact resistance.[29,30] We extracted the mobility from the saturation transfer characteristics according to the procedure developed by Di Pietro *et al.* which allows taking into account the dependence of the effective mobility on the gate voltage.[29] Average mobility values under different annealing conditions (from three different devices) are reported in Fig. 4c for the polymer P2 (a similar result is obtained in the case of P1). The organic semiconductor is either dried in a vacuum oven at room temperature (as-cast) or annealed at the corresponding temperature for 15 minutes before further processing. Mobility at low gate voltages is highly dependent on the processing conditions, however in all cases it saturates to a very similar value of 0.2 $cm^2 V^{-1} s^{-1}$. This is further shown in the case of P1 prepared on different substrates and using different annealing profiles. Top contact bottom gate (TCBG) devices on OTS treated Si/SiO_2 substrates show a constant mobility in the range of 0.3–0.4 $cm^2 V^{-1} s^{-1}$ at all gate voltages regardless of the chosen solvent. BCTG samples prepared on solvent cleaned glass substrates and annealed at 300 °C, on the other hand, show a much stronger charge density dependent mobility which is more influenced by the preparation conditions and is always very low at low charge density. The effect can be mitigated if the sample is first dried at 100 °C for 2 minutes

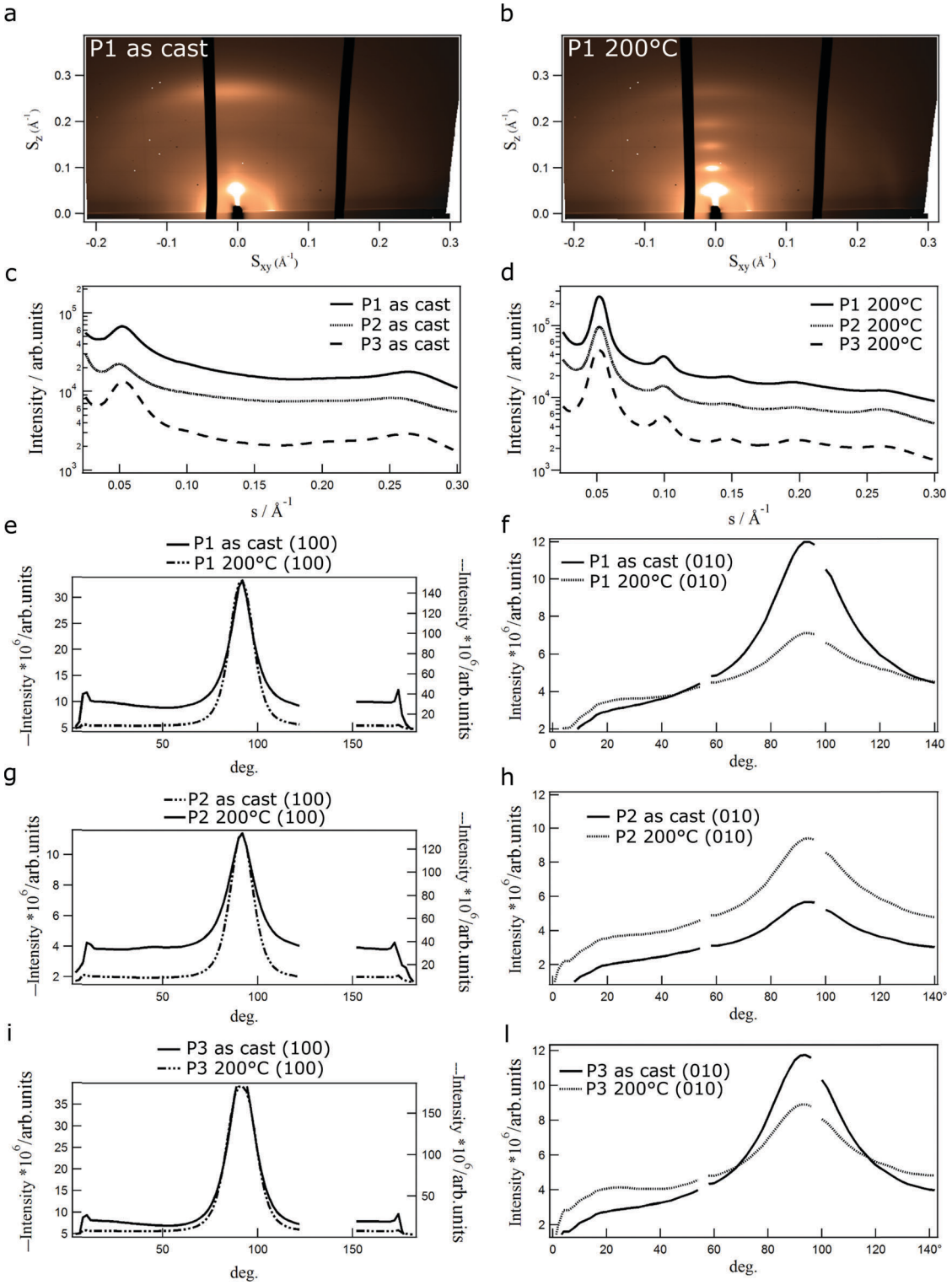

Fig. 2 2D GIWAXS patterns corresponding to deposited films of P1, as-cast and annealed at 200 °C are reported in panels a and b. Panels c and d give meridional profiles extracted from the 2D diffractograms of the as-cast and annealed films, respectively, for P1 (solid line), P2 (dotted line) and P3 (dashed line). Panels e, g and i and f, h and l display azimuthal intensity distributions corresponding to reflection 100 (e, g and i) and 010 (f, h and l) of P1, P2 and P3 samples respectively. The solid lines stand for the as-cast film and dashed-dotted and dotted lines for the film annealed at 200 °C.

before increasing the temperature up to 300 °C (slow annealing) and if OTS treated glass is used instead of bare glass. The wide range of processing conditions explored in order to optimize the device performance in all cases leads to a mobility that saturates to the same values measured in TCBG transistors with SiO_2 dielectric with OTS treatment (0.4 $cm^2 V^{-1} s^{-1}$). Mobility in

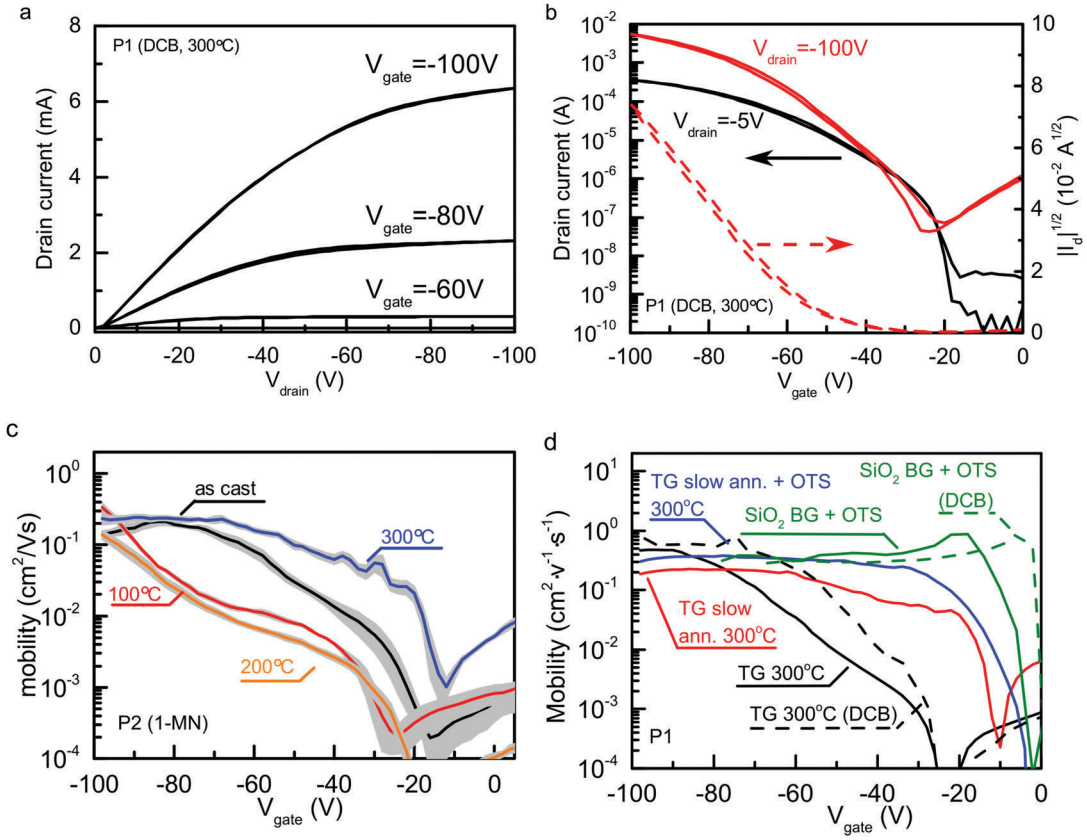

Fig. 3 (a and b) The output and transfer characteristics, respectively, of a BCTG DCB coated P1 transistor, annealed at 300 °C. The hole mobility of BCTG transistors using P2 dissolved in 1-MN under different annealing conditions is compared in (c), while the hole mobility of BCTG transistors prepared using P1 dissolved in 1-MN (solid line) and DCB (dashed line) is compared in (d) against TCBG transistors using SiO_2 with OTS coating as a dielectric. In panel c, the grey error margin resulted from the mean standard deviation of the mobility obtained from three different devices under each preparation conditions.

our high molecular weight polymer does not seem to be dependent on the choice of solvent or device geometry, contrary to what has been observed on other polymers where spin coating from high boiling point solvents usually leads to improved morphology and higher electrical performance.[19,31]

The similar mobility at high gate voltages for as-cast and annealed devices (Fig. 3c) seems to be at odd with the observation of increased crystallite size and improved crystallite orientation observed in the GIWAXS measurements upon annealing. At the same time the wide range of extracted mobilities at low gate voltages under different preparation conditions (Fig. 3d) does not seem to correlate with changes in the texture of the film, but might be induced by strong trapping effects either in the channel or in the bulk of the semiconductor. The former would be directly responsible for a decrease in mobility while the latter would be responsible for a dramatic reduction in the charge injection efficiency. Both would however show as an apparent charge density dependent mobility, strongly decreasing with decreasing charge density.[30]

Effects of air exposure

In order to get a complete picture of the charge transport properties of P(DPP2OD-TT) it proves very useful to look at the effect of air exposure. Several reports in the literature show that DPP based polymers have good stability in an ambient environment, with mobilities equal to if not higher than the ones of devices prepared in an inert atmosphere. In our experiments we found that the hole mobility of transistors prepared from P2 and P3 without any thermal annealing was 0.02 $cm^2\ V^{-1}\ s^{-1}$ for P2 and 0.001 $cm^2\ V^{-1}\ s^{-1}$ for P3 at $V_G = -70$ V (Fig. 4a, the polymer film in this case is deposited from chloroform solution). The lower calculated mobility at high gate voltages compared to the devices reported in Fig. 3 is caused by the thicker and lower capacitance dielectric of the devices prepared in IAPP (C_i = 2.0 nF cm^{-2}) compared to the one used in the devices prepared at the University of Potsdam (C_i = 6.4 nF cm^{-2}).[16] When the apparent mobility is strongly dependent on either charge density or the electric field (Fig. 3), the thicker dielectric used for the devices in Fig. 4a and b will require a much higher voltage in order to reach similar working conditions (charge density or electric field) used in the devices in Fig. 3. Device performance is however strongly improved if the semiconducting layer is spincoated from a solution that is prepared and heated in an ambient atmosphere (Fig. 4b). P2 shows a mobility of 0.4 $cm^2\ V^{-1}\ s^{-1}$ and a high on–off ratio of 10^5, in line with the one measured on annealed devices prepared with PMMA dielectric and high boiling point solvents. The very low off-current indicates that the improvement is not

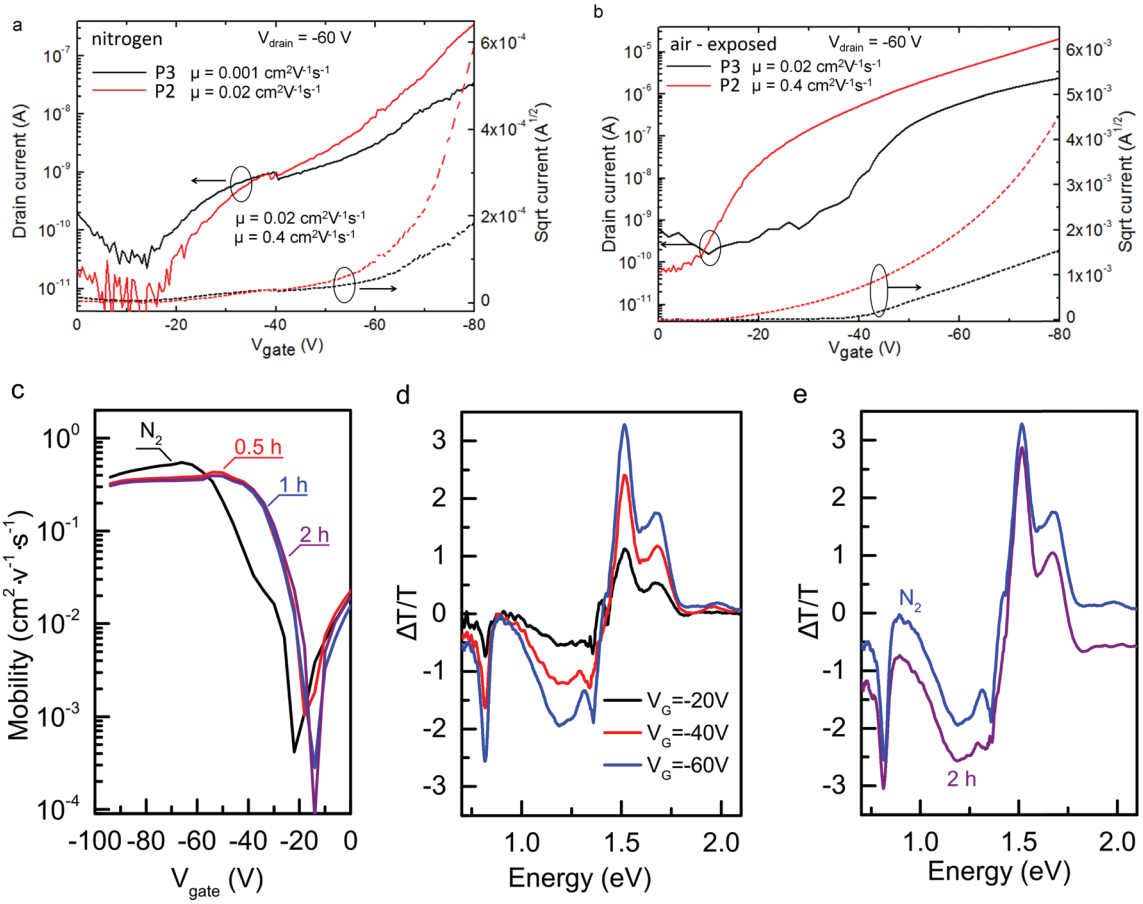

Fig. 4 (a) Transfer characteristics of P2 and P3 transistors based on P(DPP2OD-TT) fabricated completely under air-free conditions; (b) transfer characteristics of air exposed P2 and P3 transistors. (c) Evolution of charge carrier mobility upon air exposure for a P1 BCTG device coated from 1-MN; (d) CAS spectrum of the same device at different gate voltages showing the characteristic negative and positive peaks associated with polaron induced absorption and bleaching of the neutral transition respectively; (e) comparison of the CAS signal for $V_{gate} = -60$ V before and after air exposure. The two traces have been offset for clarity.

caused by air induced bulk doping of the polymer film but rather due to the passivation of electron donating trap sites present in the film. P3 shows a reduced mobility of 0.02 $cm^2 V^{-1} s^{-1}$, which in conjunction with the results of X-ray and UV-Vis characterization provides a further proof that entanglement and the hindered formation of a uniform edge-on texture might be responsible for the reduced device performance.

An analogous effect is observed when a BCTG device made by P1 coated from 1-MN and annealed at 300 °C is exposed to air after device preparation in an inert atmosphere (Fig. 4c). The device is first characterized in nitrogen and then exposed to air for 0.5, 1 and 2 hours. Upon air exposure a dramatic increase in mobility at low gate voltages is observed, quickly saturating to the maximum value of 0.4 $cm^2 V^{-1} s^{-1}$ already at $V_G = -40$ V. It is interesting to notice that while the characterization is performed in nitrogen, in one case, the solution is exposed to air before device fabrication (Fig. 4b), while in the other the device is prepared without air exposure at any stage and only exposed to air after the device fabrication is completed (Fig. 4c). This is a strong indication that either water or oxygen has the capability to passivate an electron donor defect which is present already in the pre-aggregated solution, and would eventually function as a hole trap in the polymer film.

In order to gain further information on the nature of these trapping sites we also performed charge accumulation spectroscopy (CAS) measurements on the same field-effect transistor characterized in and exposed to air, as shown in Fig. 4c.[32] CAS measures the changes in the transmission coefficient of the device upon accumulation of charge carriers. When a charge is added to a molecule the strong electrostatic interaction with the atoms of the molecule induces a rearrangement of the molecular orbitals that leads to the formation of new optical transitions.[33] These are the negative peaks at 0.82 eV and 1.20 eV in the CAS spectra in Fig. 4d, which appear together with a positive peak representing the bleaching of the neutral molecule optical transition. It is important to note that the bleaching signal shows a very strong low energy peak at 1.52 eV and only a small contribution from a higher energy peak at 1.68 eV, a clear indication that despite the presence of a large fraction of poorly aggregated and amorphous polymer chains in the polymer film, charges selectively accumulate in the most extended and planar aggregates present in the film. The comparison of CAS spectra

recorded at different gate voltages (Fig. 4d) further shows that charges accumulated on aggregated polymer chains even at $V_{gate} = -20$ V, corresponding to very low measured mobility, and that there is no spectral difference between the spectra at $V_{gate} = -20$ V, $V_{gate} = -40$ V and $V_{gate} = -60$ V. This indicates that at all gate voltages the majority of charges (>95%, up to the sensitivity level of the experimental setup) accumulate at the same electronic sites, and there is no evidence of two different species being present in the polymer film. This is extremely important since it rules out the possibility of the extrinsic trapping effect in the channel of the transistor as a possible reason for the decrease in mobility at low gate voltages. Such high density of trap states should show up in the CAS spectrum either as a nonlinear dependence of the intensity on gate voltage or as features with different spectral signatures.[29] In order to explain the observed charge density dependence of the mobility with the presence of traps in the channel a trap density comparable with the accumulated charge density would in fact be required, which is not compatible with the results of the charge accumulation spectroscopy measurements. This is demonstrated by the CAS spectrum recorded at $V_{gate} = -60$ V before and after air exposure (Fig. 4e). Except for a minor electro-absorption feature at 1.35 eV which disappears after exposure, there is no difference in the CAS spectrum both in the peak position and in their intensity, implying that charges accumulate in the same electronic environment both before and after air exposure. Having ruled out the trapping effects in the channel of the transistor, the improvement in the measured mobility must come from an improvement in the injection process. We have already shown that in staggered devices such a process is determined by both the injection process at the metal–organic semiconductor interface and due to the bulk of the polymer film on which charges have to cross in order to reach the channel.[29] We have also demonstrated that in such devices contact resistance is affected by the presence of traps in the bulk with density far lower than the charge density achieved in the channel of the device.[29]

CAS is not sensitive to trapping effects in the bulk because the lower charge density in this region of the polymer film falls below the sensitivity level of the instrument, although the electro-absorption signal might be an indication of charges being trapped in extrinsic, optically inactive sites. Therefore, we can conclude that the measured mobilities 0.4 $cm^2 V^{-1} s^{-1}$ and 0.2 $cm^2 V^{-1} s^{-1}$ for P1 and P2, respectively, are charge density independent. The increase in molecular weight from P1 to P2 seems to have a limited impact on charge transport (although the X-ray characterisation shows better morphology for P1 especially after annealing) and it is obvious that the lower aggregation and better solubility of P1 and P2 lead to highly improved transistor performance compared to the higher molecular weight batch P3. These results and the ones of UV-Vis and GPC analyses clearly indicate that the molecular weight distribution of P1 and expecially P2 is already the maximum value that leads to high charge transport performance. Higher molecular weights (such as in P3) show the onset of entanglement, a steep increase in aggregation and a reduction of solubility that are responsible for a dramatic reduction in performance.

Effect of doping on transistor performance (IAPP)

The results presented so far demonstrate how the poor charge transport properties at low gate voltages are most likely caused by trapping effects in the bulk of the polymer film, and that the improvement upon air exposure is caused by the passivation of such trapping sites. To strengthen this conclusion, in the next section, we will show that a comparable improvement in transistor performance can be attained in BCTG by doping of the P(DPP2OD-TT) by molecular dopants with no need for complex annealing or silanization steps.

Herein, we used F_6TCNNQ as the molecular dopant (Chart 1), which was recently shown to be a promising p-dopant for organic semiconductors because of its relatively low LUMO level of about −5.3 eV, as accessed by cyclic voltammetry (CV) in good agreement with the published value, electronic properties which are very close to those of F_4TCNQ (Fig. S8 and Table S1, ESI†).[34,35] It has already been shown in the literature that a significant improvement of the mobility can be obtained in P3HT/PS blends atop which an ultra-thin layer of highly electron-deficient F_4TCNQ is evaporated.[36] By blending F_4TCNQ in substantial concentrations with P3HT (HOMO level of −4.9 eV) the conductivity increased up to 6 orders of magnitude compared to the neat P3HT. We have recently reported the characterisation of the doping process for P(DPP(6-DO)$_2$TT) which shows how both F_4TCNQ and F_6TCNNQ do not have a sufficiently deep LUMO level to efficiently dope the polymer. Both P(DPP(6-DO)$_2$TT) and P(DPP2OD-TT), within the experimental error of CV characterisation, have the same HOMO energy of −5.5 eV (Fig. S9 and Table S1, ESI†). This is expected since the two polymers share the same backbone chemical structure and differ exclusively for the side chains, and will lead to a rather similar interaction with the dopant molecule.[37]

In our study, ultra-thin films of F_6TCNNQ, of nominal thickness 1 and 2 nm, were evaporated on top of the undoped P2 layer prior to the deposition of the gate insulator. Recent results have shown that evaporating F_4TCNQ on top of PBTTT leads to bulk doping due to the high diffusivity of the dopant molecule in the polymer film, rather than pure interfacial doping.[38] As can be observed, in our case, doping produces a very similar effect to air exposure, enhancing the current and showing a linear dependence of the square root of the saturation current *versus* gate voltage already at low gate voltages. The hole mobility of the transistor with p-doped P2 layers, extracted from the saturation transfer curves in Fig. 5, can reach values up to 1.2 $cm^2 V^{-1} s^{-1}$ stable over a wide gate voltage range. This manifests itself as a positive threshold voltage shift upon doping (−35 V for 1 nm F_6TCNNQ layer and 0 V for 2 nm F_6TCNNQ layer). The improvement in current and the quadratic response to the gate bias suggest the same electron donating trap passivation in the bulk of the polymer film observed upon air exposure. A trapping site for holes will in fact have higher energy than the HOMO of P(DPP2OD-TT), so that the dopant F_6TCNNQ will necessarily be more efficient in passivating electron donating trap sites than in doping P(DPP2OD-TT).[39]

The suppression of the current on–off ratio ($<10^3$) in the case of the 2 nm thick dopant layer, however, indicates the

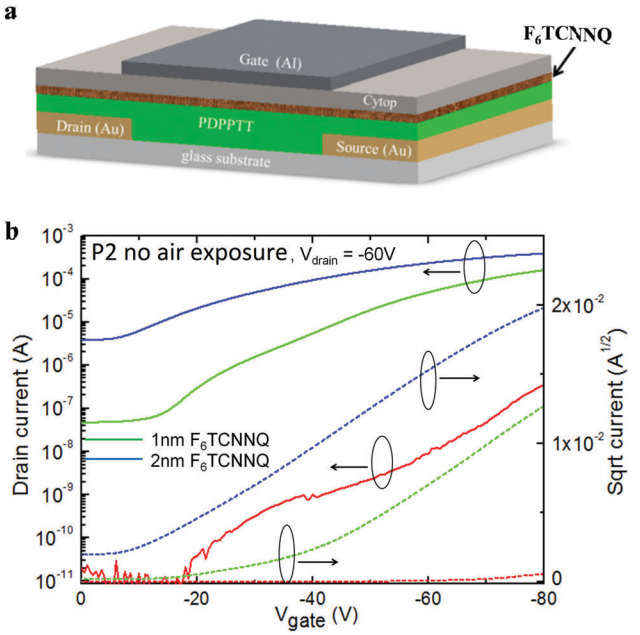

Fig. 5 (a) Schematics of the field effect transistors used for the doping study highlighting the deposition of the dopant layer at the interface with the dielectric. (b) Transfer characteristics of P2 transistors with the p-dopant layer (1 nm and 2 nm) between P(DPP2OD-TT) and the dielectric (red curve represents the intrinsic device, which acts as the comparison here).

presence of doped polymer units in the bulk that cannot be fully depleted by reversing the gate bias. Although the LUMO of F_6TCNNQ (−5.3 eV) is higher in energy compared to the HOMO level of P(DPP2OD-TT) (−5.5 eV), so that no doping would take place, this increase in bulk conductivity is in line with what was shown in ref. 37, where a limited doping of P(DPP(6-DO)$_2$TT) was observed also in combination with F_4TCNQ. It is worth noting that no further changes in the transfer characteristics of the P2 transistor are observed when the polymer semiconductor is doped by a 3 nm F_6TCNNQ layer, again supporting the limited doping efficiency of F_6TCNNQ in P(DPP2OD-TT), related to the non-optimal energy offset. The mechanism for p-type doping of a low HOMO level polymer such as P(DPP2OD-TT) with F_6TCNNQ and similar dopants is the subject of ongoing investigation.[37] The results however demonstrate a method to selectively passivate the trapping sites in a semiconducting polymer film through the optimal choice of the dopant molecule. This is a very interesting approach that could be followed to improve the reliability and performance of organic semiconductors.

Summary and conclusions

We analysed three high molecular weight batches of P(DPP2OD-TT) to understand the limiting factors for the charge transport properties of the polymer. We obtained a limit weight average molecular weight $M_w \approx 220$ kg mol^{-1} through the Stille coupling reaction (commonly used to achieve high molecular weights) beyond which the polymer solubility in chlorinated solvents is dramatically decreased due to strong aggregation phenomena, preventing the formation of uniform films. Such strong pre-aggregation in solution has a detrimental impact on the charge transport properties due to the onset of chain entanglement that hinders the formation of well-ordered polymer crystallites.[40] A comprehensive optimization of the device performance on both TCBG and BCTG transistors shows however that in P(DPP2OD-TT) the observed gate voltage dependence of the hole field effect mobility is caused by trapping in the bulk of the polymer film rather than a genuine dependence on charge density. In these high molecular weight polymer batches the improvement of the polymer film texture upon annealing seems not to be correlated with an increase of mobility but rather responsible for a reduction of traps in the bulk of the polymer film.

We further show that these traps can be efficiently passivated either by exposure to air or by modifying the injecting contact, for example, by evaporating gold on top of the organic semiconductor. Starting from such observations we demonstrate a procedure for improving charge injection into the channel of a P(DPP2OD-TT) transistor using a dopant, F_6TCNNQ, which does not have the optimal energy offset to dope the organic semiconductor but is nevertheless able to efficiently passivate the trapping sites. This improvement in device performance is obtained regardless of the molecular weight of P(DPP2OD-TT). With such procedure we achieved a significant improvement of the measured currents up to two orders of magnitude higher than the corresponding undoped devices, with a shift of the threshold voltage from −35 V to 0 V, while retaining the switching capability of the transistor. A more careful tuning of the dopant type and the evaporation process should enable the observation of the intrinsic FET mobility (not hindered by the poor injection) at low gate voltages without a significant increase in the off current we observe in our devices.

These observations shine light on the complex interplay between morphology, charge trapping and molecular doping in DPP based semiconductors, pointing out several issues that need to be considered when studying the charge transport properties of DPP polymers. While the nature of the trapping mechanism is still to be fully understood, our results clearly show how to control and passivate the trapping sites in order to improve device performance. Further studies are being planned to understand the nature of such trapping sites in order to further tune the doping mechanism, to achieve the best compromise between charge transport and on–off ratio of working transistors and obtain information on the intrinsic charge transport properties of DPP polymers.

Acknowledgements

We gratefully acknowledge support from the German Excellence Initiative *via* the Cluster of Excellence EXC 1056 "Center for Advancing Electronics Dresden" (CFAED) and DFG (grant KI-1094/9). M. A. H. thanks The University of Jordan and Leibniz-Institut für Polymerforschung, Dresden (IPF) for financial support. Dimitri A. Ivanov, David Doblas and Kirill L. Gerasimov thank

the Ministry of Education and Science of the Russian Federation for financial support (contract No 14.604.21.0121 (RFMEFI60414X0121)). The authors are grateful to O. Konovalov from the ID10 beamline of the European Synchrotron Radiation Facility (ESRF) in Grenoble (France) for excellent technical support during the synchrotron experiments.

References

1 A. C. Arias, J. D. MacKenzie, I. McCulloch, J. Rivnay and A. Salleo, *Chem. Rev.*, 2010, **110**, 324.
2 A. N. Sokolov, B. C.-K. Tee, C. J. Bettinger, J. B.-H. Tok and Z. Bao, *Acc. Chem. Res.*, 2012, **45**, 361.
3 P. M. Beaujuge and J. M. J. Frechet, *J. Am. Chem. Soc.*, 2011, **133**, 20009.
4 A. Facchetti, *Chem. Mater.*, 2010, **23**, 733.
5 K.-J. Baeg, M. Caironi and Y.-Y. Noh, *Adv. Mater.*, 2013, **25**, 4210.
6 Y. Li, P. Sonar, L. Murphy and W. Hong, *Energy Environ. Sci.*, 2013, **6**, 1684.
7 H. Sirringhaus, *Adv. Mater.*, 2014, **26**, 1319.
8 S. Holliday, J. E. Donaghey and I. McCulloch, *Chem. Mater.*, 2014, **26**, 647.
9 C. B. Nielsen, M. Turbiez and I. McCulloch, *Adv. Mater.*, 2013, **25**, 1859.
10 I. Kang, H. J. Yun, D. S. Chung, S. K. Kwon and Y. H. Kim, *J. Am. Chem. Soc.*, 2013, **135**, 14896.
11 M. M. Wienk, M. Turbiez, J. Gilot and R. A. J. Janssen, *Adv. Mater.*, 2008, **20**, 2556.
12 L. Bürgi, M. Turbiez, R. Pfeiffer, F. Bienewald, H.-J. Kirner and C. Winnewisser, *Adv. Mater.*, 2008, **20**, 2217.
13 Y. Li, S. P. Singh and P. A. Sonar, *Adv. Mater.*, 2010, **22**, 4862.
14 X. Zhang, L. J. Richter, D. M. DeLongchamp, R. J. Kline, M. R. Hammond, I. McCulloch, M. Heeney, R. S. Ashraf, J. N. Smith, T. D. Anthopoulos, B. Schroeder, Y. H. Geerts, D. A. Fischer and M. F. Toney, *J. Am. Chem. Soc.*, 2011, **133**, 15073.
15 Z. Chen, M. J. Lee, R. S. Ashraf, Y. Gu, S. Albert-Seifried, M. M. Nielsen, B. Schroeder, T. D. Anthopoulos, M. Heeney, I. McCulloch and H. Sirringhaus, *Adv. Mater.*, 2012, **24**, 647.
16 J. Li, Y. Zhao, H. S. Tan, Y. Guo, C.-A. Di, G. Yu, Y. Liu, M. Lin, S. H. Lim, Y. Zhou, H. Su and B. S. Ong, *Sci. Rep.*, 2012, **2**, 754.
17 H. N. Tsao, D. M. Cho, I. Park, M. R. Hansen, A. Mavrinskiy, D. Y. Yoon, R. Graf, W. Pisula, H. W. Spiess and K. Müllen, *J. Am. Chem. Soc.*, 2011, **133**, 2605.
18 Y. Karpov, W. Zhao, I. Raguzin, T. Beryozkina, V. Bakulev, M. Al-Hussein, L. Häußler, M. Stamm, B. Voit, A. Facchetti, R. Tkachov and A. Kiriy, *ACS Appl. Mater. Interfaces*, 2015, **7**, 12478.
19 J. Chang, J. Clarck, N. Zhao, H. Sirringhaus, D. W. Breiby, J. W. Andreasen, M. M. Nielsen, M. Giles, M. Heeney and I. McCulloch, *Phys. Rev. B: Condens. Matter Mater. Phys.*, 2006, **74**, 115318.
20 I. McCulloch, A. Salleo and M. Chabynic, *Science*, 2016, **352**, 1521.
21 C. M. Cardona, W. Li, A. E. Kaifer, D. Stockdale and G. Bazan, *Adv. Mater.*, 2011, **23**, 2367.
22 (*a*) J. Kettle, M. Horie, L. A. Majewski, B. R. Saunders, S. Tuladhar, J. Nelson and M. L. Turner, *Sol. Energy Mater. Sol. Cells*, 2011, **95**, 2186.
23 B. C. Schroeder, C. B. Nielsen, Y. J. Kim, J. Smith, Z. Huang, J. Durrant, S. E. Watkins, K. Song, T. D. Anthopoulos and I. McCulloch, *Chem. Mater.*, 2011, **23**, 4025.
24 J. W. Rumer, S.-Y. Dai, M. Levick, L. Biniek, D. J. Procter and I. McCulloch, *J. Polym. Sci., Part A: Polym. Chem.*, 2013, **51**, 1285.
25 F. C. Krebs, R. B. Nyberg and M. Jorgensen, *Chem. Mater.*, 2004, **16**(7), 1313.
26 K. T. Nielsen, K. Bechgaard and F. C. Krebs, *Macromolecules*, 2005, **38**(3), 658.
27 J. R. Matthews, W. Niu, A. Tandia, A. L. Wallace, J. Hu, W.-Y. Lee, G. Giri, S. C. B. Mannsfeld, Y. Xie, S. Cai, H. H. Fong, Z. Bao and M. He, *Chem. Mater.*, 2013, **25**, 782.
28 F. C. Spano and C. Silva, *Annu. Rev. Phys. Chem.*, 2014, **65**, 477.
29 R. Di Pietro, D. Venkateshvaran, A. Klug, E. J. W. List-Kratochvil, A. Facchetti, H. Sirringhaus and D. Neher, *Appl. Phys. Lett.*, 2014, **104**, 193501.
30 R. Di Pietro, D. Fazzi, T. B. Kehoe and H. Sirringhaus, *J. Am. Chem. Soc.*, 2012, **134**, 14877.
31 A. Luzio, L. Criante, V. D'Innocenzo and M. Caironi, *Sci. Rep.*, 2013, **3**, 3425.
32 R. Di Pietro and H. Sirringhaus, *Adv. Mater.*, 2012, **24**, 3367.
33 P. J. Brown, H. Sirringhaus, M. Harrison, M. Shkunov and R. H. Friend, *Phys. Rev. B: Condens. Matter Mater. Phys.*, 2001, **63**, 125204.
34 M. L. Tietze, L. Burtone, M. Riede, B. Lüssem and K. Leo, *Phys. Rev. B: Condens. Matter Mater. Phys.*, 2012, **86**, 035320.
35 B. Lüssem, M. Riede and K. Leo, *Phys. Status Solidi A*, 2013, **210**, 9.
36 G. Lu, J. Blakesley, S. Himmelberger, P. Pingel, J. Frisch, I. Lieberwirth, I. Salzmann, M. Oehzelt, R. Di Pietro, A. Salleo, N. Koch and D. Neher, *Nat. Commun.*, 2013, **4**, 1588.
37 Y. Karpov, T. Erdmann, I. Raguzin, M. Al-Hussein, M. Binner, U. Lappan, M. Stamm, K. L. Gerasimov, T. Beryozkina, V. Bakulev, D. V. Anokhin, D. A. Ivanov, F. Günther, S. Gemming, G. Seifert, B. Voit, R. Di Pietro and A. Kiriy, *Adv. Mater.*, 2016, **28**, 6003.
38 K. Kang, S. Watanabe, K. Broch, A. Sepe, A. Brown, I. Nasrallah, M. Nikolka, Z. Fei, M. Heeney, D. Matsumoto, K. Marumoto, H. Tanaka, S.-I. Kuroda and H. Sirringhaus, *Nat. Mater.*, 2016, **15**, 896.
39 S. Olthof, S. Mehraeen, S. K. Mohapatra, S. Barlow, V. Coropceanu, J.-L. Brédas, S. R. Marder and A. Kahn, *Phys. Rev. Lett.*, 2012, **109**, 176601.
40 R. Steyrleuthner, R. Di Pietro, B. A. Collins, F. Polzer, S. Himmelberger, M. Schubert, Z. Chen, S. Zhang, A. Salleo, H. Ade, A. Facchetti and D. Neher, *J. Am. Chem. Soc.*, 2014, **136**, 42456.

